RESEARCH   **Open Access**

On the discrete dipole approximation investigation of the extinction spectra of Ag/glass nano-flower thin film with threefold symmetry

Fatemeh Abdi, Araz Siabi-Gerjan and Hadi Savaloni[*]

Abstract

The use of glancing angle deposition technique provides opportunities for the deposition of sculptured nanostructures of different shape. The optical properties of such nanostructures that are a function of the shape of these nanostructures may be investigated, using the discrete dipole approximation theory which is an appropriate method for solving the light scattering problem from objects of different shape and geometry. In this paper, the extinction spectra of Ag/glass-sculptured nano-flowers with threefold symmetry are modeled and calculated, while the results are compared with similar experimental observations. In modeling the nano-flower-shaped sculptured thin films, it is proposed that the nano-flower is formed as a combination of two chiral thin films with different dimensions. This structure was replaced with 1,405 electrical dipoles, and its extinction spectrum was calculated as a function of incident light angle and azimuthal angle. The extinction spectrum consists of both transverse and longitudinal modes of oscillations. The results showed that by increasing the incident angle, due to increase of amplitude of electrical oscillations, transverse oscillations shift towards longer wavelengths. It was also observed that at azimuthal angles close to nano-flower petals, where sharp points or recesses may exist, the intensity of extinction spectrum for longitudinal mode (long wavelengths in the extinction spectrum) increases.

Keywords: Extinction spectra, Discrete dipole approximation, Nano-flower, Sculptured thin films, Ag/glass films

PACS: 78.67.Bf, 81.16.Rf, 78.20.Ek, 73.20.Mf, 42.79.Wc

Background

Columnar thin films (CTFs) are coatings produced by physical vapor deposition at oblique or glancing angle. In glancing angle deposition, the flux of vapor makes an angle larger than 85° with the surface normal [1]. Hence, the initially deposited adatoms on the substrate surface produce shadows at their rear area that prohibits the incoming adatoms to be accommodated in these areas; hence, growth is limited in these areas. Therefore, thin films produced with this technique contain a large fraction of voids. The ratio of voids to the deposited material may be controlled by adjustment of the incident angle. In addition, in the glancing angle method, one may also rotate the substrate holder about its surface normal, using different modes of movement and produce nano-

sculptured thin films of different shapes [2-4]. Chiral nano-sculptured thin films are produced by rotation of substrate about its surface normal with a constant speed. Pitch of these chiral thin films can be varied with the deposition rate and the rotation speed of the substrate.

If we define the deposition rate with R and the rotation speed of the substrate with ω, then the pitch of the chiral (2Ω) may be obtained as the following:

$$2\Omega = R/\omega. \tag{1}$$

Also, the radius of the chiral may be varied with the incident angle. If the substrate is pre-seeded, then, according to the size of these ordered seeds on the substrate surface, one may control the radius of the chiral [3].

Nano-flower thin films are sculptured thin film structures that may be produced with two different rotation speeds of the substrate about its surface normal (ω_1, ω_2) in

* Correspondence: savaloni@khayam.ut.ac.ir
Department of Physics, University of Tehran, North-Kargar Street, Tehran 14345-546, Iran

$2N$ sections of one complete rotating period. N defines the order of symmetry in the nano-flower structure. There should be a considerable difference between these two rotating speeds. The high speed produces a section of chiral with small dimension (stem of the nano-flower), while the low speed produces a section of chiral with large dimension (petal of the nano-flower) [5,6].

Zhao et al. [5] used glancing angle deposition of Si at 85° while they also changed the rotation rate of the substrate $2N$ ($N = 1$ to 5) times during each revolution of the substrate. In this way, they managed to change the lateral shape of the growing columns and produced nanostructures with N-fold symmetry called nano-flowers.

Savaloni et al [6] produced and characterized silver nano-flowers with different symmetries and investigated their optical spectra using both s- and p-polarizations at different azimuthal and incident angles. Some of their experimental results are used in this work for comparison [6].

Metallic nanostructures with specific properties dependent on their size and geometrical shape have created an interesting research environment for scientist in different fields of application such as biomedicine [7-12], antibacterial [13], and optics [14-16].

Nanostructures of noble metals (gold, silver, and copper), because of their ability in exhibiting localized surface plasmon resonances [17], have found many applications, particularly in the field of plasmonics [18-21]. These nanostructures may be used as substrates in surface-enhanced vibrational spectroscopy, such as the surface-enhanced Raman spectroscopy (SERS) [22-24], the surface-enhanced infrared absorbance spectroscopy [25], and metal-enhanced fluorescence spectroscopy [26-28], as well as chemical and biological sensors [29-34].

Experiments have demonstrated that the plasmon peak depends strongly on the morphology and assembly of the nanoparticles, such as diameter [18], aspect ratio [35], shape [36,37], or assembly of array and the lattice parameters of the array [38] and the dielectric constant of the host medium [39-41]. Experimental and theoretical investigations have shown that increased number of corners or recesses in the morphology of the nanostructure provides higher number of sites for creation of enhanced fields which facilates SERS detection [42].

In this work, our aim is to compare the optical spectra of Ag/glass nano-flowers with $3N$ symmetry obtained using both s- and p-polarizations at different azimuthal and incident angles with the results of calculations using discrete dipole approximation (DDA). This work is, to the best of our knowledge, the first of its kind to be reported on the DDA results for the nano-flowers which is successfully modeled, and its results are consistent with those of experimental ones, while one should consider the differences between the experiment and the model. It is also worthwhile to mention that the results reported in this

paper are preliminary achievements and further calculations with higher number of dipoles, and perhaps, refinement of the model may be required.

Experimental details

Silver nano-flower-shaped sculptured thin films with threefold symmetry were deposited on glass (15×15 mm^2 microscope slide) substrates by resistive evaporation from tungsten boats at room temperature. The purity of silver was 99.99 %. An Edwards (Edwards E19 A3, West Sussex, UK) coating plant with a base pressure of 3×10^{-7} mbar was used. The deposition angle was fixed at 75°, and a deposition rate of 2.5 s^{-1} was chosen. Figure 1 shows the schematic of the evaporation system showing substrate position and rotation for sculptured thin film growth. The distance between the evaporation source and the substrate was 30 cm. In order to provide a point source for geometrical considerations, a plate of tungsten with a 6-mm diameter hole in the middle was used as a mask on top of the evaporation boat. The deposition process was repeated a few times, and the reproducibility of the results was confirmed. The movement of the stepper motor and its speed of revolution, as well as facility for dividing each revolution to different sectors, are controlled through interface to a computer in which the related software is written and installed. All these are domestic made.
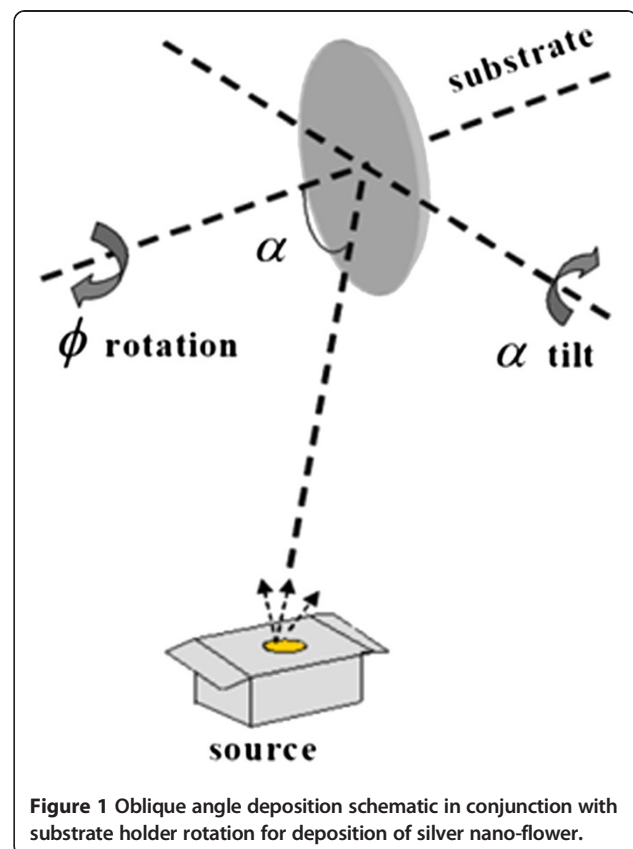

Figure 1 Oblique angle deposition schematic in conjunction with substrate holder rotation for deposition of silver nano-flower.

Nano-flowers with threefold symmetry were produced; considering that for an N-fold symmetry, each revolution of the substrate holder should be divided to $2N$ sectors. In this work, the smaller sector was chosen as ($\Theta_L = 24°$) which rotates with a speed of $R_L = 0.0151$ rev/s, while the other sectors size depends on the order of chosen symmetry and its speed (R_H) was chosen to be 32 times that of R_L.

Prior to deposition, all substrates were ultrasonically cleaned in heated acetone and then ethanol. The surface roughness of the substrates was measured by a Talysurf profilometer (Taylor Hobson, Leicester, England, UK) and atomic force microscope, and the root mean square substrate surface roughness R_q obtained using these methods were 0.3 and 0.9 nm, respectively.

The deposition rate was measured by a quartz crystal deposition rate controller (SQM-160, Sigma Instruments, Cranberry Township, PA, USA) positioned close to the substrate and at almost the same azimuthal angle as that of the substrate. This was corrected after obtaining the film thickness using field emission electron microscopy (FESEM) (S-4100 SEM, Hitachi High-Tech, Minato-ku, Tokyo, Japan). FESEM samples were coated with a very thin layer of gold to prevent the charging effect. The surface physical morphology and roughness was obtained by means of atomic force microscopy (AFM) (Solver, NT-MDT, Moscow, Russia, with a Si tip of 10 nm radius in non-contact mode) analysis. Reflectance and transmittance spectra of the samples were obtained using a single beam spectrophotometer (nkd-8000, Aquila Instruments, Essex, UK) in the spectral range of 350 to 1,050 nm using both s- and p-polarization measurements in steps of 5 nm.

Silver nano-flower structural characteristics

FESEM images of the silver nano-flower-shaped sculptured thin film with threefold symmetry are given in Figure 2. Figure 2a shows the surface structure of this film around a defect. This defect has acted as a natural shadowing block (pre-grown seed), and the threefold symmetry can be clearly observed in this image. Figure 2b is a larger scale image from the surface structure of this film. The symmetry of the grown nano-flowers on the surface of the films is shown by geometrical shapes (i.e., triangles) while the orientation of grown arms/columns (directions/petals) are also shown by black arrows. These arrows show the principal axes that the columns grow along their directions. Figure 2c shows the cross section of silver nano-flowers. Due to high surface diffusion of silver adatoms, the initial temperature of the substrate (room temperature), and the heat accumulation during the long time deposition of these sculptured thin films (approximately 5 h), and the fact that films were grown on bare (unseeded) glass substrates, the pitches of the chiral shapes are not clearly distinguishable. However, more careful examination of these cross sections not only shows the chirality of the grown films, but also
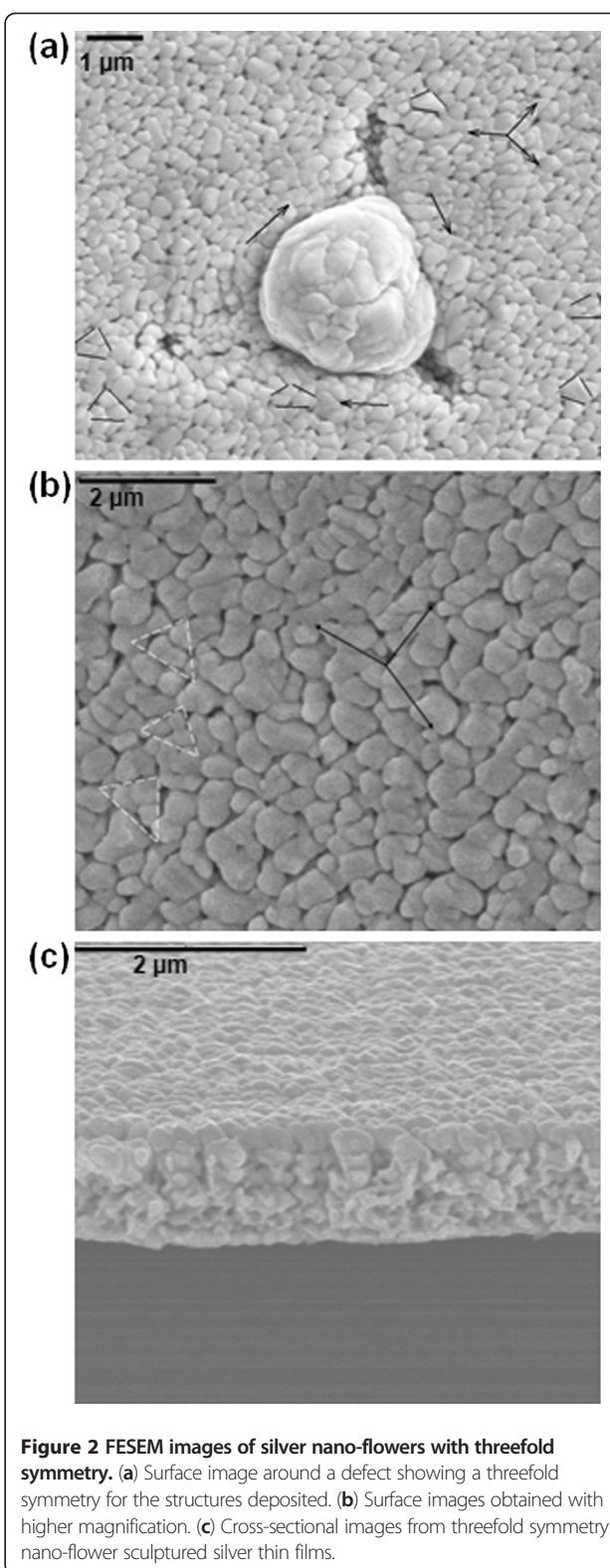

Figure 2 FESEM images of silver nano-flowers with threefold symmetry. (**a**) Surface image around a defect showing a threefold symmetry for the structures deposited. (**b**) Surface images obtained with higher magnification. (**c**) Cross-sectional images from threefold symmetry nano-flower sculptured silver thin films.

some petals of the nano-flowers. It is worthwhile to mention that it was a laborious and cumbersome task to obtain such cross-sectional images from these samples. The

diameter of the vertical columns/chirals including the width of petals may be estimated as approximately 300 nm while the columnar/chiral stem itself (excluding the petals) is about approximately 50 nm. Zhao et al. [5] who grow Si nano-flowers on Si(100) substrates with cooling facility for the substrate to keep the substrate temperature fixed at 4°C during deposition also encountered such difficulty, while diffusion of Si adatoms on the Si substrate is much less than Ag adatoms on glass substrates. In addition, as mentioned above, they also used the cooling facility for the substrate while the temperature during our deposition of Ag films (which took a considerably long time) increased above room temperature (i.e., initial substrate temperature).

If the pre-seeding is arranged in a way that seeds are in a sufficient distance from each other, then the neighboring columns will not affect each other [5]. If neighboring nuclei are close to each other, then one may shadow the other one; hence, nano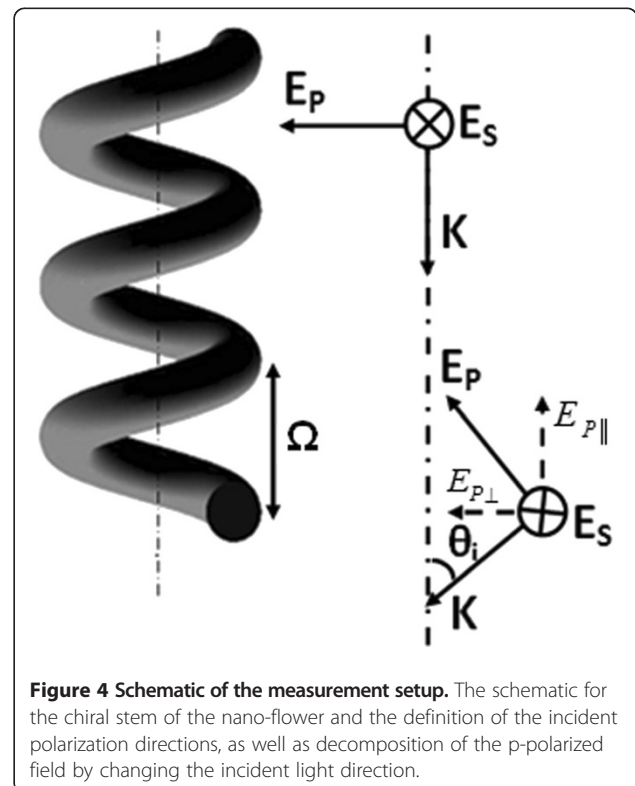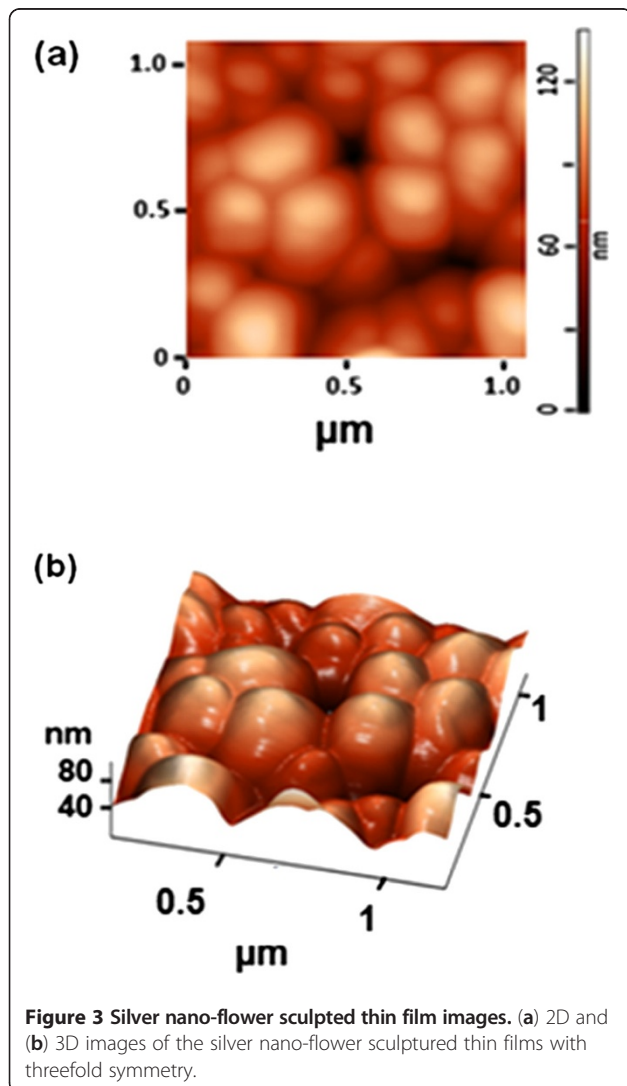-flowers with missing one or few petals may result. The latter has been the case for our samples that were grown on flat microscope slides.

In Figure 3, two-dimensional (2D) and three-dimensional (3D) AFM images of silver nano-flowers of threefold symmetry are given. These images clearly show the threefold symmetry nano-flowers. Size distributions of the grains/petals of these nano-flowers were obtained from the 2D AFM images using JMicroVision Code (University of Geneva, Geneva, Switzerland) as 92 nm.

Experimental optical spectra of Ag/glass nano-flowers

Transmission and reflection spectra of silver nano-flower-shaped sculptured thin films with threefold symmetry were measured in the wavelength region of 350 to 1,050 nm at two different incident angles of 30° and 70°, and at different azimuthal angles (φ) of 0°, 45°, 90°, 135°, and 180°, for both s- and p-polarizations. Figure 4 shows the schematic of the measurement setup. We define the p-polarization at the plane of grown nano-flowers and the s-polarization at normal to this plane. In Figure 4, only the chirality of the nano-flower structure is shown, and the grown petals on this structure are omitted for clarity.

In obtaining the absorption/extinction spectra from our optical measurements, the following effects/phenomenon were considered: (a) the transmittance spectrum from our nano-flower silver thin films was negligible due to the high film thickness; (b) usually, the non-specular reflection is very low for Ag films, and it is also well known that by

Figure 3 Silver nano-flower sculpted thin film images. (**a**) 2D and (**b**) 3D images of the silver nano-flower sculptured thin films with threefold symmetry.

Figure 4 Schematic of the measurement setup. The schematic for the chiral stem of the nano-flower and the definition of the incident polarization directions, as well as decomposition of the p-polarized field by changing the incident light direction.

increasing the particle size, the absorption maximum shifts towards lower energies and the band/peak becomes broader; (c) it is also possible that higher order modes become excited; and (d) in case of particles whose size is smaller than the wavelength of the incident light, the electromagnetic wave cannot distinguish their structural details. However, the absorption spectrum may be affected by their shape. When features with different shapes are distributed in the structure of thin films, they cause broadening of the absorption peaks. If the feature size is about the same or greater than the wavelength of the incident light, then scattering becomes the dominant process in the extinction spectrum (i.e., absorption + scattering) [43]. Hence, according to the AFM results, since the size of our nano-flowers is smaller than the minimum wavelength (i.e., 350 nm), it may be concluded that the scattering contribution in our work is negligible. Therefore, it may be a good approximation to consider (1-R) as the film extinction which may show the surface plasmon resonances in the Ag nanostructures.

The incident angle is also an important parameter in plasmon excitation [44]. The 70° incident angle was chosen to make sure that the p-polarized light interacts with the Ag column with almost its maximum electric field, while the 30° incident angle should provide information from the nano-flower surface morphology, including anisotropy when the φ angle is changed.

In Figure 4, it is shown that when the incident light interacts with the nano-flower at an angle, the E_p field decomposes into two components: a field parallel to ($E_{p\text{II}}$) and a field perpendicular to ($E_{p\perp}$) the long axis of the Ag rod. Therefore, the larger θ_i results in larger $E_{p\text{II}}$ component.

Hence $E_{p\text{II}}$ excites the longitudinal mode (LM), and $E_{p\perp}$ excites the transverse mode (TM) [29].

Figure 5 shows the (1-R) (as explained above, this may be considered as extinction with good approximation) spectra of the threefold symmetry nano-flower for p-polarization measured at 30° incident angle and different φ angles (ranging from 0° to 180° in steps of 45°), respectively.

A common peak at about 350 nm (which can be distinguished with some difficulty due to our limitation for the measurement at the lower wavelengths) and a broad peak at about 391 to 406 nm for the p-polarized light corresponding to the transverse plasmon mode resonances (TM) can be distinguished. These peaks are directly related to the nano-columns topography. The common peak at about 350 nm is called the transverse quadrupole mode (TQM), and the peak located at longer wavelength is called transverse dipole mode (TDM) [45,46]. In addition, a very broad shoulder can be observed.

Figure 6 shows the (1-R) spectra of the threefold symmetry nano-flower of p-polarization measured at 70° incident angle. The distinguished feature in these spectra is the broad shoulder (peak) at higher wavelengths, which have higher intensity than that observed for 30° incident angle. Zhao et al. [29] also found a very broad shoulder similar to that observed in this work for aligned Ag nano-rod arrays prepared by oblique angle deposition particularly when the film thickness is more than 600 nm (see Figure 5a in the work of Zhao et al. [29]). Our nano-flowers are not perfectly aligned structures (see FESEM pictures in Figure 2) though majority of them are aligned in one direction, but there is a distribution. In addition, when the incident light
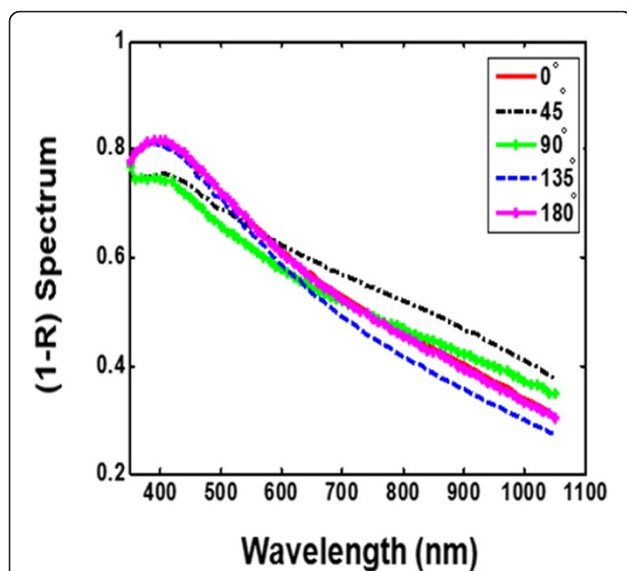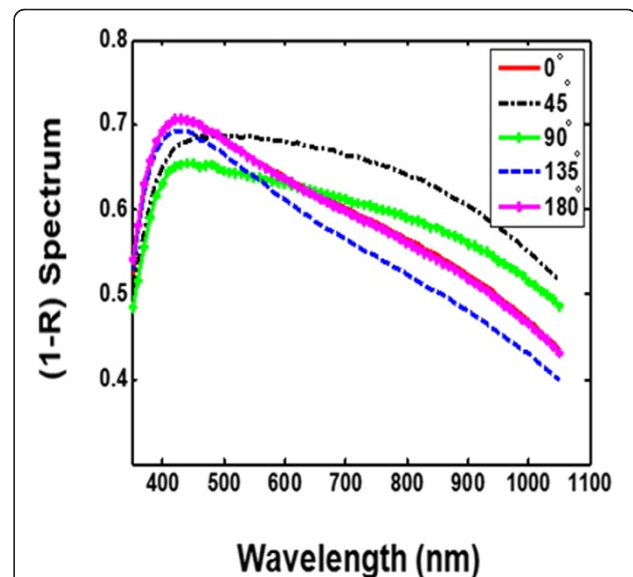
Figure 5 (1-R) Spectra of Ag 3N chiral nano-flower thin film. These spectra were obtained at 30° incident angle for p-polarization light and different azimuthal angles.

Figure 6 (1-R) Spectra of Ag 3N chiral nano-flower thin film. These spectra were obtained at 70° incident angle for p-polarization light and different azimuthal angles.

has an angle with respect to the long axis of nano-flower, then as discussed above (Figure 4), the E_p field will be decomposed into two components: a field parallel to (E_{pII}), and a field perpendicular to ($E_{p\perp}$) the Ag nano-flower long axis. Therefore, E_{pII} excites the LM plasmon mode, and $E_{p\perp}$ excites the TM plasmon mode. Hence, when the incident angles of 30° and 70° are compared, the E_{pII} (LM plasmon mode) of the latter is stronger and contributes to the broad shoulder at higher wavelengths. As it can be deduced from Figure 4 and the above discussion, p-polarization can excite all plasmon modes.

DDA theory

Since the exact solution of the Maxwell equation only exists for a certain number of geometries, there is a need for other methods to obtain the optical properties of nanoparticles with arbitrary geometrical shapes. DDA method is a useful technique for solving light scattering problems from objects with arbitrary geometries. In this theory, the object is in arbitrary shape, but its size is of the order of wavelength or smaller than the wavelength of the incident light [47,48]. This object is then replaced with an array of point dipoles, and the interaction of these dipoles with the electric field of the incident light is considered. The dipoles, because of electric field, react with each other, too. Therefore, the applied/external electric field produces a local electric field at a position of each point dipole; in addition, the rest of the dipoles also produce an electric field at this point. Hence, each dipole effectively consists of an electrical dipole momentum due to the local electric field of the process just mentioned. Therefore, calculation of this dipole momentum will provide the appropriate facility for obtaining answers to the scattering problems [49,50]. For larger objects, one should also consider the high multipolar excitations [51]. The distance between dipoles, d, in the array can be obtained as follows:

$$V = Nd^3$$
$$d = (V/N)^{\frac{1}{3}},$$

(2)

where N is the number of point dipoles and V is the volume of the object. In order to solve this problem by replacing the object with an assembly of point dipoles, both the position of N dipoles (r_i, $i = 1, \ldots, N$) and dipole momentums P_i must be determined. When this dipole momentum is determined, one can calculate the absorption, scattering, and extinction cross sections of light. According to the Clausius-Mossotti equation, polarizability of an electrical dipole i, at a position r_i with a dielectric constant of ϵ_i, is given as follows [52]:

$$\alpha_i^{CM} = \frac{3d^3}{4\pi} \frac{\epsilon_i - 1}{\epsilon_i + 2}.$$

(3)

Since the radiation interaction effects are not considered in Equation 3, the Clausius-Mossotti equation does not satisfy the energy conservation law. Hence, inclusion of radiation interaction effects modifies Equation 3, and the polarizability of the electrical dipole is as follows [49,50]:

$$\alpha_i = \frac{\alpha_i^{CM}}{1 - (2/3)ik^3 \alpha_i^{CM}}.$$

(4)

In Equation 4, α_i^{CM} is the Clausius-Mossotti polarizability, and k is the wave number. Electrical dipole momentum is then obtained as follows:

$$p_i = \alpha_i . E_{loc}(r_i).$$

(5)

In Equation 5, $E_{loc}(r_i)$ is the local electric field (i.e., the electrical field at the position of ith dipole) which is the sum of the incident electric field and the electric field due to the rest of point dipoles in the suggested array for the object under examination [53]:

$$E_{loc}(r_i) = E_{inc,i} - \sum_{j \neq i} A_{ij} P_j,$$

(6)

where E_{inc} is the incident electric field. If E_{inc} is a plain wave field with a wave number k, then by omitting its time dependence, its dependence on the position is as follows:

$$E_{inc}(r) = E_0 \exp(ik.r).$$

(7)

P_i is the electrical dipole momentum of ith dipole, and A_{ij} is the vector potential that is given as [53] follows:

$$A_{ij} = \frac{\exp(ikr_{ij})}{r_{ij}}$$
$$\times \left[k^2 (\hat{r}_{ij}\hat{r}_{ij} - I_3) + \frac{ikr_{ij} - 1}{r_{ij}^2} (3\hat{r}_{ij}\hat{r}_{ij} - I_3) \right],$$

(8)

where $r_{ij} = r_i - r_j$, $\hat{r}_{ij} = \frac{r_i - r_j}{|r_i - r_j|}$, and I_3 is a 3×3 identity matrix. Using the definition $A_{ii} = \alpha_i^{-1}$, the electrical dipole momentum may be obtained as follows:

$$\sum_{j=1}^{N} A_{ij} p_j = E_{inc,i}.$$

(9)

One can then calculate the absorption, scattering, and extinction cross sections as follows:

$$C_{ext} = \frac{4\pi k}{|E_0^2|} \sum_{i=1}^{N} Im\left(E_{inc,i}^* . P_i \right),$$

(10)

$$C_{abs} = \frac{4\pi k}{|E_0^2|} \sum_{i=1}^{N} \left\{ Im\left[P_i . (\alpha_i^{-1})^* P_i^* \right] - \frac{2}{3} k^3 |P_i|^2 \right\},$$

(11)

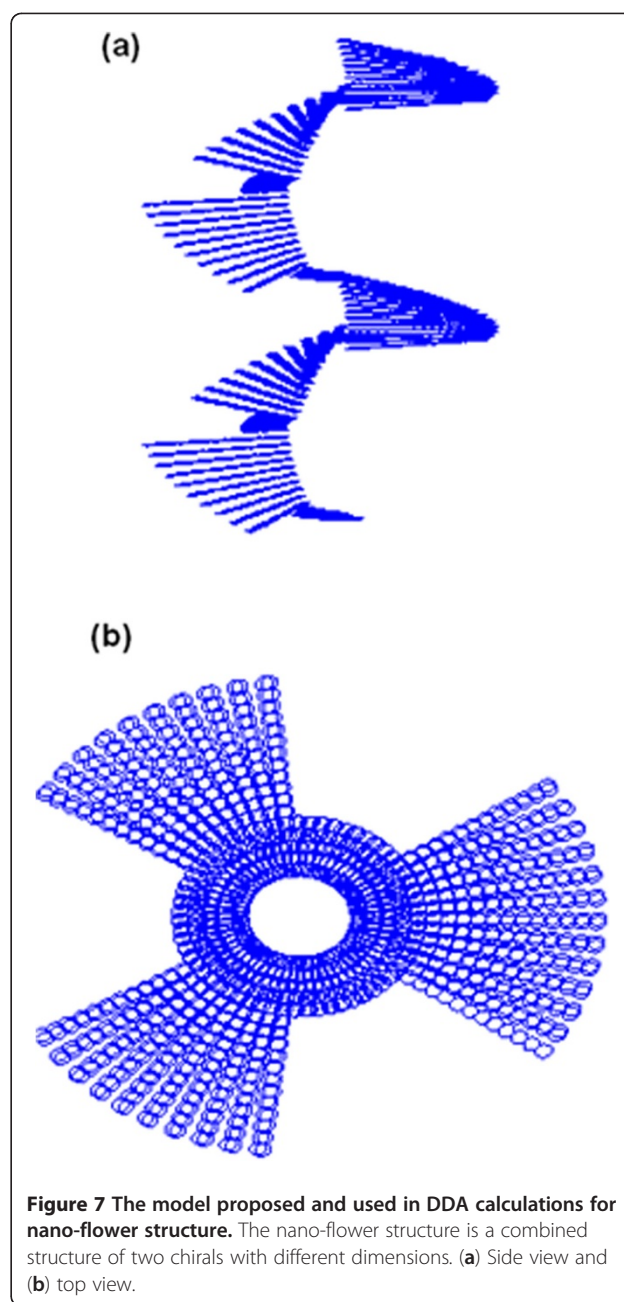$$C_{sca} = C_{ext} - C_{abs}.$$

(12)

Owing to the ability of the DDA theory in solving the scattering problem from objects of complex in different shapes, it has attracted the attention of many researches during the last few years. Sosa et al. [51] in 2003 calculated the extinction spectra for silver nanoparticles in spherical, ellipsoidal, and cubic shapes. In 2006, Zhang and Zhao [54] reported their results for extinction spectra of silver rods of different shapes (i.e., needle, periodical nano-rod, L-shaped nano-rod, and Y-shaped nano-rod). They also investigated the dependence of extinction spectra on the nano-rod height, and their results showed that extinction spectra shift towards long wavelengths with increasing the height of the nano-rod [29,55]. Later, Zhang and Zhao [56] investigated the extinction spectrum of a U-shaped silver structure with varying dimensions. Their results showed that the extinction spectra are strongly dependent on the dimensions (size) of this structure; for large scale U-shaped structure, they obtained numerous resonance peaks that increased with size. They concluded that in addition to electrical dipole effects, one should also include multiple dipole effects in the calculations [56]. They also, in another work [47], reported their findings for a silver chiral structure with varying structural parameter and azimuthal incident angle, while they compared these results with those of a multiring.

In this work, as mentioned in the 'Background' section, we report our results for extinction spectra of a threefold symmetry silver nano-flower and its variation with incident angle and azimuthal angle using the DDA theory.

The model

As mentioned before, nano-flower is a structure that may be produced by rotation of the substrate about its surface normal with two considerably different speeds at $2N$ sections of one complete rotation. Hence, it may be assumed that the nano-flower is a structure that is formed as a combined structure of two chiral structures with different dimensions. When the substrate is rotating with high speed, a section of chiral with a small dimension (stem) is formed. On the contrary, when the substrate is rotating with slow speed, a section with a large dimension (petal) is formed. In this paper, we have investigated the extinction spectra for a threefold symmetry silver nano-flower with two pitches, while each pitch is divided into six sections. Of these six sections, three sections are the petals of the nano-flower, and between them are three sections of the stem of the nano-flower. Figure 7 shows a schematic drawing of the nano-flower under investigation.

The parameters used in this DDA calculation were chosen as follows: the pitch of thin chiral is 15 nm with outer and inner radii of 25 nm and 10 nm, respectively, and the pitch of thick chiral is 150 nm with outer and inner radii of 50 nm and 10 nm, respectively. The nano-flower

Figure 7 The model proposed and used in DDA calculations for nano-flower structure. The nano-flower structure is a combined structure of two chirals with different dimensions. (**a**) Side view and (**b**) top view.

structure in Figure 7 was filled with 1,405 dipoles with a distance of 9.33 nm between them, and the extinction spectra at incident angles of 30° and 70° and at different azimuthal angles were obtained using DDA calculations.

DDA results and discussion

The extinction spectra of silver nano-flower were calculated in the wavelength region of 300 to 700 nm for p-polarization of incident light. In these spectra, both TM and LM were observed. Figure 8 shows the DDA result for extinction spectrum of the modeled nano-flower at incident angle of 70° and azimuthal angle of 180° for a
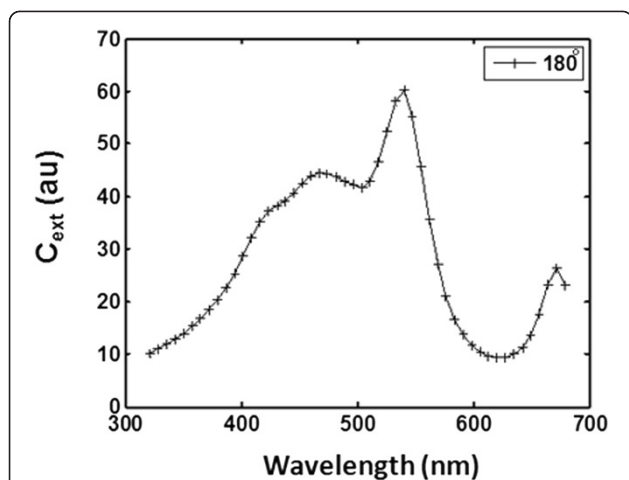
Figure 8 Result of DDA calculation of extinction spectrum for Ag 3N chiral nano-flower thin film. These were obtained at 70° incident angle and 180° azimuthal angle for p-polarization light.

p-polarized light. It can be observed that there exist four oscillation peaks. These peaks have appeared at 430-, 460-, 540-, and 670-nm wavelengths. TM is located at the 430-nm wavelength which is due to the electric field component in the chiral cross-sectional direction of the nano-flower axis, and LM mode is due to the electric field component along the chiral axis of the nano-flower which occurs at longer wavelengths (peaks at 460, 540, and 670 nm).

The number of oscillation peaks in the extinction spectrum depends on the number of directions that are possible for electronic oscillations which in turn depends on the dimensions of the nanoparticle. In Figure 9, the effect of incident angle on the extinction spectrum of the modeled nano-flower is shown. It can be observed that the
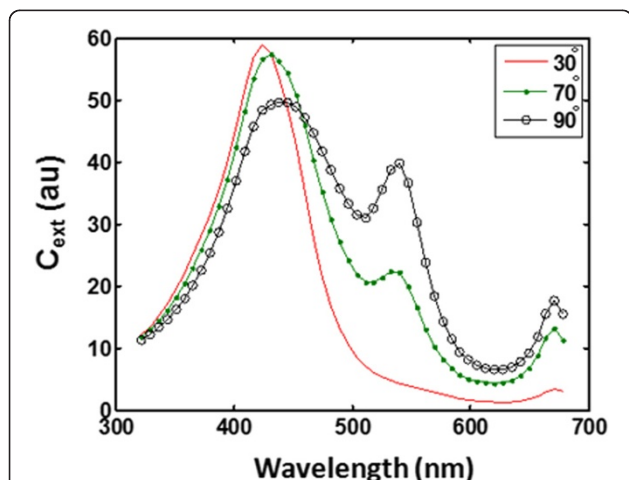
TM peak (peak that appeared at lower wavelength of about 430 nm) is gone under a redshift (i.e., longer wavelengths) with increasing incident angle. This is due to the fact (as mentioned above; Figure 4) that the $E_{p\mathrm{II}}$ becomes stronger at higher incident angles. In addition, it can also be seen that only at 70° and 90° incident angles do the LM peaks appear in the spectra, and they become stronger with increasing incident angle.

Influence of variation of azimuthal angle on the extinction spectra from the modeled nano-flower is investigated for two incident angles of 30° and 70° in Figures 10 and 11, respectively. At 30° incident angle up to 135° azimuthal angle, all spectra almost show the same behavior, though the intensity of peaks change in a way that, in general, one may suggest that when the intensity of TM peak is increased, the intensity of LM peaks decreased and vice versa. This is more pronounced in the case of 180° incident angle. The same behavior can be observed in Figure 11 for the 70° incident angle. However, much stronger LM peaks than those obtained for the 30° incident angle can be distinguished. This is again due to the fact that at this higher incident angle, as discussed above, $E_{p\mathrm{II}}$ is greater, and hence, its contribution to the LM peaks is higher than 30° incident angle.

Now, if we compare the experimental results in Figures 5 and 6 with those obtained from DDA calculations in Figures 10 and 11, in general, we can observe similarities. However, one may also claim that there exist some obvious differences. A comparison of Figure 5 (experimental results) with Figure 1 (DDA) in fact shows a great deal of agreements, though in Figure 1, the broad shoulder at long wavelengths is missing. This and other discrepancies will be explained in the following paragraphs.

A comparison of Figure 6 (experimental results) with Figure 11 (DDA) again shows good agreements. In general,
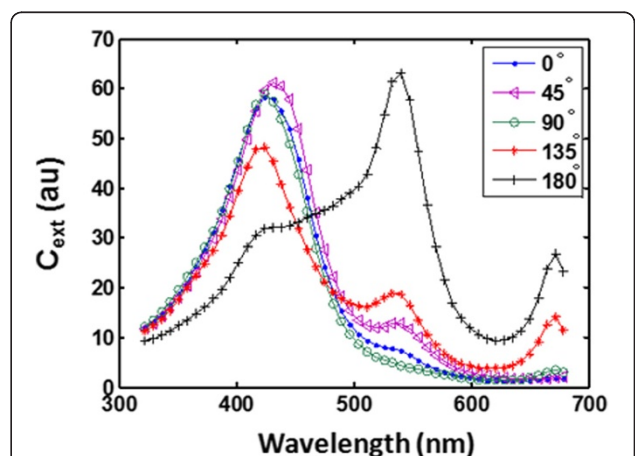

Figure 9 Result of DDA calculation of extinction spectra for Ag 3N chiral nano-flower thin film. These were obtained at different incident angles.

Figure 10 Result of DDA calculation of extinction spectra for Ag 3N chiral nano-flower thin film. These were obtained at 30° incident angle and different azimuthal angles for p-polarization light.
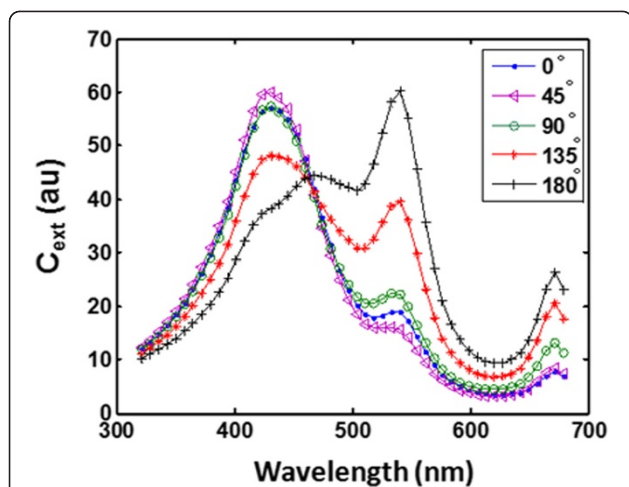
Figure 11 Result of DDA calculation of extinction spectra for Ag 3N chiral nano-flower thin film. These were obtained at 70° incident angle and different azimuthal angles for p-polarization light.

the differences observed between the experimental and DDA results can be attributed to the following parameters: (a) DDA calculations were terminated at 700 nm; hence, longer wavelength results are missing. (b) Experimental results are obtained from nano-flower thin films with seven pitches with structural parameter of 150 nm, and the ratio of high speed rotation of substrate to the low speed section was 32:1, while DDA calculations were carried out for a nano-flower with two pitches with a structural parameter of 150 nm and ratio of high to low rotation speed of 10. (c) DDA calculations were carried out for a single threefold symmetry nano-flower, while the experimental results were obtained for an assembly of nano-flowers on the substrate. (d) Our experimental nano-flowers are not perfectly aligned structures (see FESEM images in Figure 2) though majority of them are aligned in one direction, but there is a distribution. In addition, when the incident light has an angle with respect to the long axis of the nano-flower, then, as discussed above (Figure 4), the E_p field will be decomposed into two components: a field parallel to ($E_{p\text{II}}$), and a field perpendicular to ($E_{p\perp}$) the Ag nano-flower long axis. Therefore, $E_{p\text{II}}$ excites the LM plasmon mode, and $E_{p\perp}$ excites the TM plasmon mode. Hence, when the incident angles of 30° and 70° are compared, the $E_{p\text{II}}$ (LM plasmon mode) of the latter is stronger and contributes to the broad shoulder at higher wavelengths. As it can be deduced from Figure 4 and the above discussion, p-polarization can excite all plasmon modes. Therefore, it may be concluded that the broad peak at longer wavelengths in both Figures 5 and 6 is due to overlap of a few LM peaks at this region from the unaligned nano-flowers on the substrate and from those that due to shadowing effect have lost one or more of their petals or have not grown in full size. (e) The film thickness is also found to be an important parameter in the optical

spectra investigations. (f) DDA calculations were carried out using only 1,045 dipoles. This was due to our limitations on the use of computer which is planned to be improved in the near future and to carry out calculations with much higher number of dipoles while the distance between dipoles then can be adjusted. In addition, some refinements of the model can be of some importance, too.

Conclusions

DDA theory is an appropriate technique for obtaining results for light scattering from arbitrary-shaped complex objects. Silver nano-flower is modeled as a combination of two chiral sculptured structures with different dimensions. When the substrate is rotating with high speed, a section of chiral with small dimension (stem) is formed. On the contrary, when the substrate is rotating with slow speed, a section with large dimension (petal) is formed. The extinction spectra from the threefold symmetry silver nano-flower with two pitches are obtained using DDA calculations for light incident at 30° and 70° angles and at different azimuthal angles. The results are compared with those of silver nano-flowers deposited on glass substrate with seven pitches. In general, good agreements are achieved between the DDA and experimental results, though the model proposed in this work requires some further refinements, and there is a need for a higher capacity (i.e., high computational speed and memory) computer for inclusion of much greater number of dipoles in the calculations. The discrepancies between the DDA and experimental results are related to the difference in the number of pitches in two sets of results, to the fact that for DDA calculations, a single nano-flower was considered, while in the experiment, an assembly of nano-flowers are involved that may also contain some degree of misalignment and imperfection of the nano-flowers due to shadowing effects, and to the overlap of few LM peaks at longer wavelengths in the experimental spectra.

References
1. Schmidt, D, Kjerstad, A.C., Hofmann, T, Skomski, R, Schubert, E, Schubert, M: Optical, structural, and magnetic properties of cobalt nanostructure thin films: J. Appl. Phys. **105**, 113508 (2009)
2. Jensen, MO, Brett, MJ: Porosity engineering in glancing angle deposition thin films: Appl. Phys. A. **80**, 763 (2005)
3. Kennedy, SR, Brett, MJ, Toader, O, John, S: Fabrication of Tetragonal Square Spiral Photonic Crystals: Nano. Lett. **2**, 59 (2002)
4. Lakhtakia, A, Messier, R: Sculptured thin films – I Concepts. Mat. Res. Innovat. **1**, 145 (1997)
5. Zhao, YP, Ye, DX, Wang, GC, Lu, TM: Novel nano column and nano flower arrays by glancing angle deposition: Nano. Lett. **2**, 351 (2002)

6.   Savaloni, H, Haydari-Nasab, F, Malmir, M: Nano-structural characteristics and optical properties of silver chiral nano-flower sculptured thin films: Appl. Surf. Sci. **257**, 9044 (2008)
7.   Khlebtsov, BN, Khanadeyev, VA, Ye, J, Mackowski, DW, Borghs, G, Khlebtsov, NG: Coupled plasmon resonances in monolayers of metal nanoparticles and nanoshells: Phys. Rev. B. **77**, 035440 (2008)
8.   Jain, PK, Lee, KS, El-Sayed, IH, El-Sayed, MA: Calculated Absorption and Scattering Properties of Gold Nanoparticles of Different Size, Shape, and Composition: Applications in Biological Imaging and Biomedicine. J Phys Chem B **110**, 7238 (2006)
9.   Riboh, JC, Haes, AJ, McFarland, AD, Ranjit, C, Van Duyne, RP: A Nanoscale Optical Biosensor: Real-Time Immunoassay in Physiological Buffer Enabled by Improved Nanoparticle Adhesion: J. Phys. Chem. B. **107**, 1772 (2003)
10. Shafer-Peltier, KE, Haynes, CL, Glucksberg, MR, Van Duyne, RP: Toward a glucose biosensor based on surface-enhanced Raman scattering: J. Am. Chem. Soc. **125**, 588 (2003)
11. Storhoff, JJ, Elghanian, R, Mucic, RC, Mirkin, CA, Letsinger, RL: One-Pot Colorimetric Differentiation of Polynucleotides with Single Base Imperfections Using Gold Nanoparticle Probes. J. Am. Chem. Soc **120**, 1959 (1998)
12. Rosi, NL, Mirkin, CA: Nanostructures in biodiagnostics. Chem Rev **105**, 1547 (2005)
13. Pal, S, Tak, YK, Song, JM: Antimicrobial Properties of a Novel Silver-Silica Nanocomposite Material: Appl. Env. Mic. **73**, 6 (2007)
14. Pendry, JB: Playing Tricks with Light. Science **285**, 1687 (1999)
15. Maier, SA, Kik, PG, Atwater, HA, Meltzer, S, Harel, E, Koel, BE, Requicha, AG: Local Detection of Electromagnetic Energy Transport Below the Diffraction Limit in Metal Nanoparticle Plasmon Waveguides: Nat. Mater. **2**, 229 (2003)
16. Zhang, JZ: Plasmonic Optical Properties and Applications of Metal Nanostructures: Noguez. C: Plasmonics **3**, 127 (2008)
17. Zhang, ZY, Zhao, YP: Optical properties of helical Ag nanostructures calculated by discrete dipole approximation method: Appl. Phys. Lett. **90**, 221501 (2007)
18. Alivisatos, AP: Semiconductor Clusters Nanocrystals, and Quantum Dots. Science **271**, 933 (1996)
19. Andersen, PC, Rowlen, KL: Brilliant Optical Properties of Nanometric Noble Metal Spheres, Rods, and Aperture Arrays: Appl. Spectrosc. **56**, 124A (2002)
20. Bartlett, PN, Baumberg, JJ, Coyle, S, Bartlett, PN, Baumberg, JJ, Coyle, S, Abdelsalam, ME: Optical properties of nanostructured metal films. Faraday Discuss **125**, 117 (2004)
21. Flory, F, Escoubas, L: Optical properties of nano - structured thin films. Progress in Quantum Electronics. Prog. Quantum Electron **28**, 89 (2004)
22. Vo-Dinh, T: surface enhanced raman spectroscopy using metallic nano structures: Trends. Anal. Chem **17**, 557 (1998)
23. Tian, ZQ, Ren, B, Wu, DY: Surface-Enhanced Raman Scattering: From Noble to Transition Metals and from Rough Surfaces to Ordered Nanostructures: J. Phys. Chem. B. **106**, 9463 (2002)
24. Campion, A, Kambhampati, P: Surface Enhanced Raman Scattering: Chem. Soc. Rev. **27**, 241 (1998)
25. Aroca, RFR, Ross, DJ, Domingo, C: Surface-enhanced infrared spectroscopy. Appl. Spectrosc. **58**, 324A (2004)
26. Aslan, K, Lakowicz, J.R., Geddes, C.D.: advanced surfaces for metal enhanced fluorescence: J. Biophys. **88**, 374A (2005)
27. Aslan, K, Gryczynski, I, Malicka, J, Matveeva, E, Lakowicz, JR, Geddes, CD: metal enhanced fluorescence: an emerging tool in biotechnology: Curr. Opin. Biotechnol. **16**, 55 (2005)
28. Geddes, CD, Lakowicz, JRJ: Editorial Metal enhanced fluorescence. Fluoresc. **12**, 121 (2002)
29. Zhao, YP, Chaney, SB, Zhang, ZY: Absorbance spectra of aligned Ag nanorod arrays prepared by oblique angle deposition. J Appl. Phys. **100**, 063527 (2006)
30. Alivisatos, AP: The use of nanocrystals in biological detection: Nat. Biotechnol. **22**, 47 (2004)
31. Mirkin, CA, Letsinger, RL, Mucic, RC, Storhoff, J: A DNA-based method for rationally assembling nanoparticles into macroscopic materials. Nature **382**, 607 (1996)
32. Haes, AJ, Van Duyne, RP: A Unified View of Propagating and Localized Surface Plasmon Resonance Biosensors. Anal Bioanal. Chem. **379**, 920 (2004)
33. O'Neal, P, Hirsch, LR, Halas, NJ, Payne, JD, West, JL: Photo-thermal tumor ablation in mice using near infrared-absorbing nanoparticles. Cancer Lett. **209**, 171 (2004)
34. Maier, SA, Brongersma, ML, Kik, PG, Meltzer, S, Requicha, H: Plasmonics—A Route to Nanoscale Optical Devices. A. Atwater, Adv. Mater **13**, 1501 (2001)
35. Link, S, El-Sayed, MA: Spectral properties and relaxation dynamics of surface plasmon electronic oscillations in gold and silver nanodots and nanorods. J Phys. Chem. **B103**, 8410 (1999)
36. Chen, SH, Webster, S, Czerw, R, Xu, JF, Carroll, DL: Morphology effects on the optical properties of silver nanoparticles. J. Nanosci. Nanotechnol **254** (2004)
37. Mock, JJ, Barbic, M, Smith, DR, Schultz, DA, Schultz, SJ: Shape effects in plasmon resonance of individual colloidal silver nanoparticles: Chem. Phys. **116**, 6755 (2002)
38. Harfenist, SA, Wang, ZL, Whetten, RL, Vezmar, I, Alvarez, MM: Three-dimensional hexagonal close-packed superlattice of passivated Ag nanocrystals: Adv. Mater. Weinheim **9**, 817 (1997)
39. Orfanides, P, Buckner, TF, Buncick, MC, Meriaudeau, F, Ferrell, TL: Demonstration of surface plasmons in metal island films and the effect of the surrounding medium—An undergraduate experiment. Am J. Phys. **68**, 936 (2000)
40. Xu, G, Tazawa, M, Jin, P, Nakao, S, Yoshimura, K: Wavelength tuning of surface plasmon resonance using dielectric layers on silver island films: Appl. Phys. Lett. **82**, 3811 (2003)
41. Mock, JJ, Smith, DR, Schultz, S: Local refractive index dependence of plasmon resonance spectra from individual nanoparticles. Nano Lett. **3**, 485 (2003)
42. Kelly, KL, Coronado, E, Zhao, LL, Schatz, GC: The Optical Properties of Metal Nanoparticles: The Influence of Size, Shape and Dielectric Environment: J. Phys. Chem. B **107**, 668 (2003)
43. Bohren, CF, Huffman, D: R: Absorption and Scattering of Light by Small Particles. John Wiley & Sons Inc., NewYork (1983)
44. Zhao, YP, Chaney, SB, Shanmukh, S, Dluhy, RAS: Polarized surface enhanced Raman and absorbance spectra of aligned Silver nanorod arrays. J. Phys. Chem. B **110**, 3153 (2006)
45. Zhang, ZY, Zhao, YP: Optical properties of helical and multiring Ag nanostructures: The effect of pitch height: J. Appl. Phys. **104**, 013517 (2008)
46. Zong, RL, Zhao, J, Li, Q, Du, B, Fu, M, Qi, XW, Li, LT: Synthesis and optical properties of silver nanowire arrays embedded in anodic alumina membrane: J. Phys. Chem. B **108**, 16716 (2004)
47. Purcell, EM, Pennypacker, CR: scattering and absorbtion of light by nonspherical dielectric grains: J. Astrophys. **186**, 705 (1973)
48. Yang, WH, Schatz, GC, Van Duyne, RP: Discrete dipole approximation for calculating extinction and Raman intensities for small particles with arbitrary shapes: J. Chem. Phys. **103**, 3 (1995)
49. Draine, BT: The Discrete-Dipole Approximation and its Application to Interstellar Graphite Grains: J. Astrophys. **333**, 848 (1988)
50. Yurkin, MA, Hoekstra, AG: The discrete dipole approximation for simulation of light scattering by particles much larger than the wavelength: J. Quant. Spect. Rad. Trans. **106**, 558 (2007)
51. Sosa, IO, Noguez, C, Barrera, RG: Optical Properties of Metal Nanoparticles with Arbitrary Shapes: J. Phys. Chem. **B107**, 6269 (2003)
52. Draine, BT, Flatau, PJ: Discrete-dipole approximation for scattering calculations: J. Opt. Soc. Am. A. **11**, 4 (1994)
53. Lazarides, AA, Lance Kelly, K, Jensen, TR, Schatz, GC: Optical Properties of Metal Nanoparticles and Nanoparticle Aggregates Important in Biosensors. J. Molecular Structure(Theochem) **529**, 59 (2000)
54. Zhang, ZY, Zhao, YP: Tuning the optical absorption properties of Ag nanorods by their topologic shapes: A discrete dipole approximation calculation: J. Appl. Phys. **89**, 023110 (2006)
55. Zhang, ZY, Zhao, YP: Extinction spectra and electrical field enhancement of Ag nanorods with different topologic shapes: J. Appl. Phys. **102**, 113308 (2007)
56. Zhang, ZY, Zhao, Y: Optical properties of U-shaped Ag nanostructures: J. Phys. Cond. Matt. **20**, 345223 (2008)